Disclosing the Interfacial Electrolyte Structure of Na-Insertion Electrode Materials: Origins of the Desolvation Phenomenon

Kateryna Goloviznina, Ezzoubair Bendadesse, Jean-Marie Tarascon, Mathieu Salanne, Ozlëm Sel

▶ **To cite this version:**

Kateryna Goloviznina, Ezzoubair Bendadesse, Jean-Marie Tarascon, Mathieu Salanne, Ozlëm Sel. Disclosing the Interfacial Electrolyte Structure of Na-Insertion Electrode Materials: Origins of the Desolvation Phenomenon. ACS Applied Materials & Interfaces, 2023, 15 (51), pp.59380-59388. 10.1021/acsami.3c12815 . hal-04390081

HAL Id: hal-04390081
https://cnrs.hal.science/hal-04390081

Submitted on 18 Jan 2024

HAL is a multi-disciplinary open access archive for the deposit and dissemination of scientific research documents, whether they are published or not. The documents may come from teaching and research institutions in France or abroad, or from public or private research centers.

L'archive ouverte pluridisciplinaire **HAL**, est destinée au dépôt et à la diffusion de documents scientifiques de niveau recherche, publiés ou non, émanant des établissements d'enseignement et de recherche français ou étrangers, des laboratoires publics ou privés.

Distributed under a Creative Commons Attribution - NonCommercial - NoDerivatives 4.0 International License

Disclosing the interfacial electrolyte structure at Na-insertion electrode materials: origins of desolvation phenomenon

Kateryna Goloviznina,[†,‡] Ezzoubair Bendadesse,[¶,§,‡] Ozlem Sel,[¶,‡] Jean-Marie Tarascon,[¶,‡] and Mathieu Salanne[*,†,‡,‖]

†*Sorbonne Université, CNRS, Physicochimie des Électrolytes et Nanosystèmes Interfaciaux, F-75005 Paris, France*

‡*Réseau sur le Stockage Electrochimique de l'Energie (RS2E), FR CNRS 3459, 80039 Amiens Cedex, France*

¶*Chimie du Solide et de l'Energie, UMR 8260, Collège de France, 75231 Paris, Cedex 05, France*

§*Sorbonne Université, CNRS, Laboratoire Interfaces et Systemes Electrochimiques, LISE, UMR 8235, 75005 Paris, France*

‖*Institut Universitaire de France (IUF), 75231 Paris, France*

E-mail: mathieu.salanne@sorbonne-universite.fr

Abstract

Among a variety of promising cathode materials for Na-ion batteries, polyanionic Na-insertion compounds are among the preferred choice due to known fast sodium transfer through the ion channels along their framework structures. The most interesting representatives are $Na_3V_2(PO_4)_3$ (NVP) and $Na_3V_2(PO_4)_2F_3$ (NVPF), which display large Na^+ diffusion coefficients (up to $10^{-9}\,m\,s^{-2}$ in NVP) and high voltage plateaux

https://doi.org/10.26434/chemrxiv-2023-7d7tz **ORCID:** https://orcid.org/0000-0002-1753-491X Content not peer-reviewed by ChemRxiv. **License:** CC BY-NC-ND 4.0

(up to 4.2 V for NVPF). While the diffusion in the solid material is well-known to be the rate-limiting step during charging, already being thoroughly discussed in the literature, liquid-state transport of sodium ions towards the electrode was recently shown to be important due to complex ion desolvation effects at the interface. In order to fill the blanks in the description of the electrode/electrolyte interface in Na-ion batteries, we performed a molecular dynamics study of the local nanostructure of a series of carbonate-based sodium electrolytes at the NVP and the NVPF interfaces along with the careful examination of the desolvation phenomenon. We show that the tightness of solvent packing at the electrode surface is a major factor determining the height of the free energy barrier associated with desolvation, which explains the differences between the NVP and the NVPF structures. To rationalize and emphasize the remarkable properties of this family of cathode materials, a complementary comparative analysis of the same electrolyte systems at the carbon electrode interface was also performed.

1 Introduction

Being commercialized for about 25 years, Li-ion batteries (LIBs) have performed a revolution in energy-storage devices.[1–3] However, due to a constantly increasing demand in the number of devices and growth of the required performance, which is confronted by supply constraints, the development of alternatives emerges as a state-of-the-art direction of battery research. An appealing option is to use Na-ion batteries (SIBs) that possess similar characteristics as Li-based analogs, being notably cheaper thanks to the high natural abundance of sodium.[4–7] However, the transition from LIBs to SIBs brings new challenges in battery design requiring developments of the cathode and anode materials as well as adjustments in the electrolyte composition.[8,9]

NaSICON materials, which have a general formula of $Na_aM_b(XO_4)_c$ (where X = Fe, V, Ti, Zr, etc., X = S, P, Si, etc.),[10,11] being a subclass of polyanionic Na-insertion compounds,demonstrate fast Na^+ diffusion in "skeleton" structures[12] that make them powerful

https://doi.org/10.26434/chemrxiv-2023-7d7tz **ORCID:** https://orcid.org/0000-0002-1753-491X Content not peer-reviewed by ChemRxiv. **License:** CC BY-NC-ND 4.0

cathode materials for SIBs.[13] Their advantages include high redox potential due to the unique inductive effect of the polyanionic groups, high thermal stability, and robustness of the structural framework during intercalation/deintercalation processes that guarantees long life cycling, while as a main drawback, their low electrical conductivity is considered.[4,5,14] The most common representative is $Na_3V_2(PO_4)_3$ (NVP), which has a theoretical capacity of $117\,mA\,h\,g^{-1}$ and a plateau at 3.4 V corresponding to the V^{3+}/V^{4+} redox reaction.[15] Going beyond the NaSICON family, a further increase of the redox potential in the Na-insertion electrode compounds can be achieved by introducing electronegative anions, such as F^-, OH^-, etc., into the NVP, which perturb the covalent bond between the transition metal and oxygen atoms.[14] Therefore, by replacing one phosphate group with fluorine anions, forming $Na_3V_2(PO_4)_2F_3$ (NVPF), one can attain a two high voltage plateau at 3.6 V and 4.2 V.[16]

The choice of the electrolyte remains crucial for the performance of SIBs.[17–19] The most common way is to use a solution of sodium salt in an organic solvent, following the strategy of LIBs, though flammability and lack of safety stay an issue.[20] A typical example is a $NaPF_6$, $NaClO_4$, or $NaBF_4$ salt dissolved in a carbonate solvent. Cyclic carbonates such as propylene carbonate (PC) or ethylene carbonate (EC) have a relatively high dielectric constant that favors the dissociation of a salt, while their linear analog such as dimethyl carbonate (DMC) are often used as co-solvents to reduce the viscosity and ameliorate ionic conductivity of a system.[21] The carbonates remain the first choice also because of the formation of a highly stable solid-electrolyte interphase (SEI) that protects anode from the direct interaction with the solution.[7,22] Alternatively, ionic liquids[23] and aqueous[24] electrolytes can be used, but they do not lack disadvantages: the ILs usually possess high viscosities compared to conventional organic solvents that tend to increase even further upon the addition of a salt,[25] while the aqueous electrolytes have a narrow voltage stability window.[26]

While the majority of studies focus on the Na^+ diffusion in the Na-insertion materials and the unit cell breathing upon intercalation,[27–33] the cathode-electrolyte interfacial structure remains underinvestigated. Nevertheless, the arrangement of the solvent at the electrode sur-

https://doi.org/10.26434/chemrxiv-2023-7d7tz **ORCID:** https://orcid.org/0000-0002-1753-491X Content not peer-reviewed by ChemRxiv. **License:** CC BY-NC-ND 4.0

face affects ion desolvation and its migration from the bulk toward the interface, known to be an important energy-consuming step.[34,35] For example, the energy barrier of Li^+ desolvation in an interphase-free $LiPF_6$/EC-DMC/$Li_4Ti_5O_{12}$ measured by electrochemical impedance spectroscopy reaches about $12\,kcal\,mol^{-1}$.[36] Of course, extensive experimental studies are barely possible for scanning a vast range of electrolyte compositions combined with different electrode types, and theoretical methods such as classical molecular dynamics (MD) are indispensable for the rational design of electrode-electrolyte systems.[37]

In recent work, we combined electrochemical quartz crystal microbalance and operando infrared fiber evanescent wave spectroscopy with MD to study the operation of Na-insertion materials-based SIBs.[38] We showed that upon insertion, a depletion of desolvated Na^+ occurs at the interface, which can impact the rate capability of the batteries, and may be generic to other types of solvent/ionic species.[39] Here we complement this work through the use of extensive MD simulations. We shed light on the local structure of 1 M $NaPF_6$ electrolyte in several organic carbonates (DMC, PC, and EC-DMC mixture (1:1 by molar fraction)) at the NVP and NVPF electrode surfaces, which will be compared to that at a graphite electrode. Note that although SIBs generally employ hard carbon as the anode, the local structure of graphite provides a good model for the interface with the electrolyte. We demonstrate that the packing of a solvent at an electrode surface due to solvent-electrode interactions appears as one of the determining factors defining the activation barrier of the desolvation process.

2 Methods

Molecular dynamics simulations were performed using the LAMMPS program.[40] Initial configurations and input files were generated using Packmol,[41] VESTA[42] and fftool[43] utilities. The simulation box consisted of two electrodes, separated by a 1 M solution of $NaPF_6$ in DMC, EC-DMC (1:1 molar fraction) or PC solvent. As electrode sets, graphite-graphite, NVP-Au and NVPF-Au pairs were considered. In total, 9 different systems were modelled.

https://doi.org/10.26434/chemrxiv-2023-7d7tz **ORCID:** https://orcid.org/0000-0002-1753-491X Content not peer-reviewed by ChemRxiv. **License:** CC BY-NC-ND 4.0

An example of a simulation box is given in Figure 1.

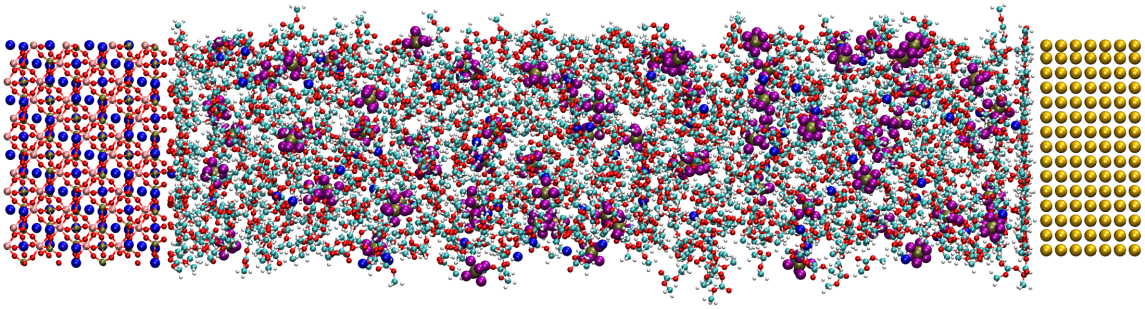

Figure 1: Simulation snapshot of the 1 M $NaPF_6$/DMC electrolyte in contact with the NVP (left) and gold (right) electrodes.

The graphite electrode (GR) was represented by a hexagonal P 6 3/m m c space group[44] and consisted of 3 layers of 34.08×36.89 Å size each. The NVP electrode was represented by a rhombohedral R -3 c space group, which is mostly always been reported in the literature,[45–47] though Masquelier *et al.*[27,33] mention several times the existence of a monoclinic distortion at ambient temperature. The slab had a size of 34.92 × 30.24 × 21.65 Å. The [001] plane of NVP was exposed toward the solution, following the recommendations from the literature.[27] The crystal structure of the NVP comprised two types of Na^+ ions, shown in Figure 2a, the occupancy of which varied from one reference to another.[27,45–47] In order to match the experimental composition, we removed Na1 and Na2 ions only from the bulk of the electrode and not from the surface, which allowed us to avoid the intercalation of Na^+ ions from the solution to the solid. The NVPF electrode was represented by a tetragonal P 42/m n m space group,[48] with the [001] plane exposed towards the solution, similarly to the NVP case. The slab had a size of 36.19 × 36.19 × 19.96 Å. The crystal structure contained two types of Na^+ ions, with the occupancy of 1.0 for Na1 and 0.5 for Na2, respectively (Figure 2b (left)). Since the distance of the closest Na2 sites is too short (1.865 Å), two neighboring Na2 sites cannot be simultaneously occupied due to the strong Coulomb repulsion between Na^+ ions.[49] Therefore, we had to remove half of Na2 atoms from the NVPF surface, and the resulting structure is given in Figure 2b (right). In all cases, a gold counter-electrode was

https://doi.org/10.26434/chemrxiv-2023-7d7tz **ORCID:** https://orcid.org/0000-0002-1753-491X Content not peer-reviewed by ChemRxiv. **License:** CC BY-NC-ND 4.0

used. It was represented by a cubic Fm-3m space group[50] with the [100] plane exposed to the solvent. The slab had a thickness of 12.22 Å, while its x and y dimensions were adjusted to fit those of NVP or NVPF.

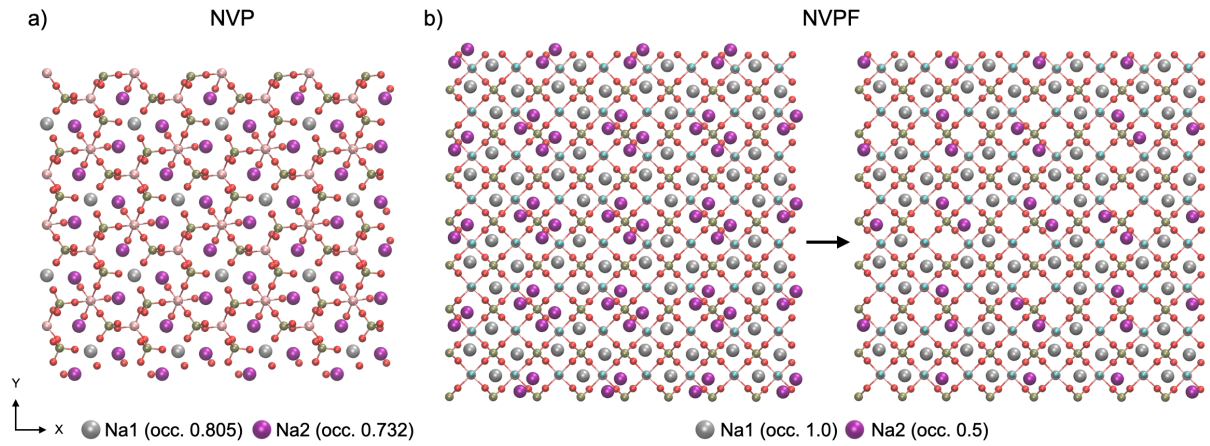

Figure 2: Visualisation of the NVP (a) and NVPF (b) surfaces exposed to a solution. Grey and purple spheres represent the Na^+ ions with different occupation (denoted as Na1 and Na2). In the case of NVP, no Na1 and Na2 ions were removed from the surface. Instead, they were removed from the bulk electrode to match the corresponding occupation (not shown). In the case of NVPF, all Na1 ions were kept, and one of Na2 in each pair (b, left) was removed for the surface (b, right).

The liquid phase contained 75 ion pairs of $NaPF_6$ salt and 845 molecules of DMC, 830 molecules of PC or [465 molecules of DMC plus 465 molecules of EC], matching the 1 M salt concentration. The box size in z direction was adjusted based on the electrode type used, resulting in a 100–120 Å solution thickness. The total system size was approximately 15 000 atoms.

The Na^+ cation was represented by Aqvist force field,[51] while the parameters of the PF_6^- anion were taken from the CL&P model.[52,53] The net charge of the ions was kept integer. The intermolecular interaction parameters of the electrode atoms, given in Table 1, were considered from several sources.[19,51,54–57] The bonded and non-bonded parameters of solvent atoms were taken from the OPLS-AA,[58] except for the partial charges, which were computed using the CHelpG procedure[59] on electron densities obtained at the MP2/cc-pVTZ level of theory at previously optimized geometries with the Gaussian16 program.[60]

https://doi.org/10.26434/chemrxiv-2023-7d7tz ORCID: https://orcid.org/0000-0002-1753-491X Content not peer-reviewed by ChemRxiv. License: CC BY-NC-ND 4.0

The solvent models were validated by computing the densities and viscosities of bulk 1 M $NaPF_6$ solutions in the DMC, EC-DMC, and PC systems, which were compared to the experimental values.

Table 1: Non-bonded interaction parameters of electrodes

Electrode	Atom type	q / e$^-$	σ / Å	ϵ / kJ mol^{-1}	Ref.
Graphite	C	0	3.330	0.2300	54
NVP, NVPF	Na	+1	3.330	0.0120	51
	V	+3	2.673	0.0602	55
	P	+5	3.740	0.1400	56
	O	−2	3.150	0.1700	56
	F	−1	3.440	0.4600	57
Gold	Au	0	2.951	22.1334	19

The simulation box was periodic in the x and y directions and a slab of $3 \times L_z$ was considered along the z direction. A cutoff of 12 Å was applied for non-bonded interactions. The particle-particle particle-mash (PPPM) method was used to evaluate electrostatic energies (the accuracy of 10^{-5}), with the slab correction taken into account. Both electrodes were considered immobile. Bonds terminating with hydrogen atoms were constrained using the SHAKE algorithm. The time step was set to 1 fs. The Nosé-Hoover thermostat was used to keep the temperature of the electrolyte solution at 298 K. Each system was equilibrated for 5 ns in the NVT ensemble and then a 50 ns production run was performed. The data analysis was performed using TRAVIS[61,62] and our self-written tools. The visualization of the simulation box was done in VMD.[63]

The potentials of mean force (PMF) were calculated from separate runs, during which a single Na^+ ion was pulled from the solution towards the electrode surface. For this, a harmonic biasing potential varying between 25 kcal mol^{-1} Å^{-2} and 150 kcal mol^{-1} Å^{-2} was applied to this Na^+ ion. The z distance between the ion and the top surface atoms (C for graphite and Na for NVP and NVPF) was considered as the biasing collective variable. It was sampled between 12 Å and −2 Å with a step of 0.25 Å with 100 ps equilibration and 400 ps acquisition at each separation. The PMFs were calculated using the umbrella sampling and

https://doi.org/10.26434/chemrxiv-2023-7d7tz **ORCID:** https://orcid.org/0000-0002-1753-491X Content not peer-reviewed by ChemRxiv. **License:** CC BY-NC-ND 4.0

the weighed-histogram analysis method (WHAM).[64,65]

From the PMF trajectories, the coordination numbers of Na^+ as a function of its distance to an electrode were calculated. The coordination number cutoff was set to 4.55 Å for P of PF_6^- and 3.20 Å for O atoms of the carbonyl group of carbonate molecules, being defined as the position of the first minimum of the corresponding radial distribution functions of bulk systems. The coordination number curves were averaged over 3–6 replicas.

3 Results and discussion

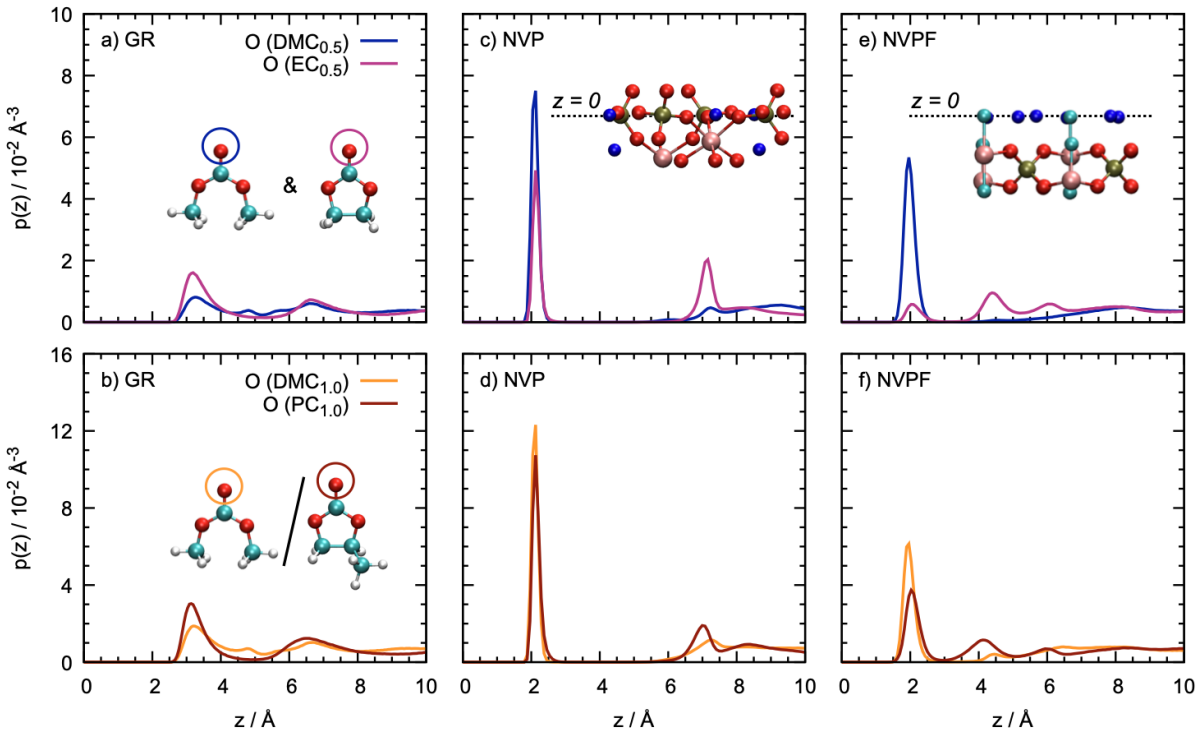

Figure 3: Density profiles of O atoms (of the C=O carbonyl group) of solvents in 1 M solution of $NaPF_6$ in the EC-DMC mixture (a,c,e) and DMC, PC solvents (b,d,f), as a function of their distance from the graphite (a,b), NVP (c,d), and NVPF (e,f) electrodes. As a reference ($z = 0$), the top carbon layer of graphite and the top sodium ions of the NVP and NVPF are considered, as illustrated by the inset.

We first analyze the structure adopted by the solvent molecules at the various interfaces. Density profiles (Figure 3), which provide information on the probability of finding species as

https://doi.org/10.26434/chemrxiv-2023-7d7tz ORCID: https://orcid.org/0000-0002-1753-491X Content not peer-reviewed by ChemRxiv. License: CC BY-NC-ND 4.0

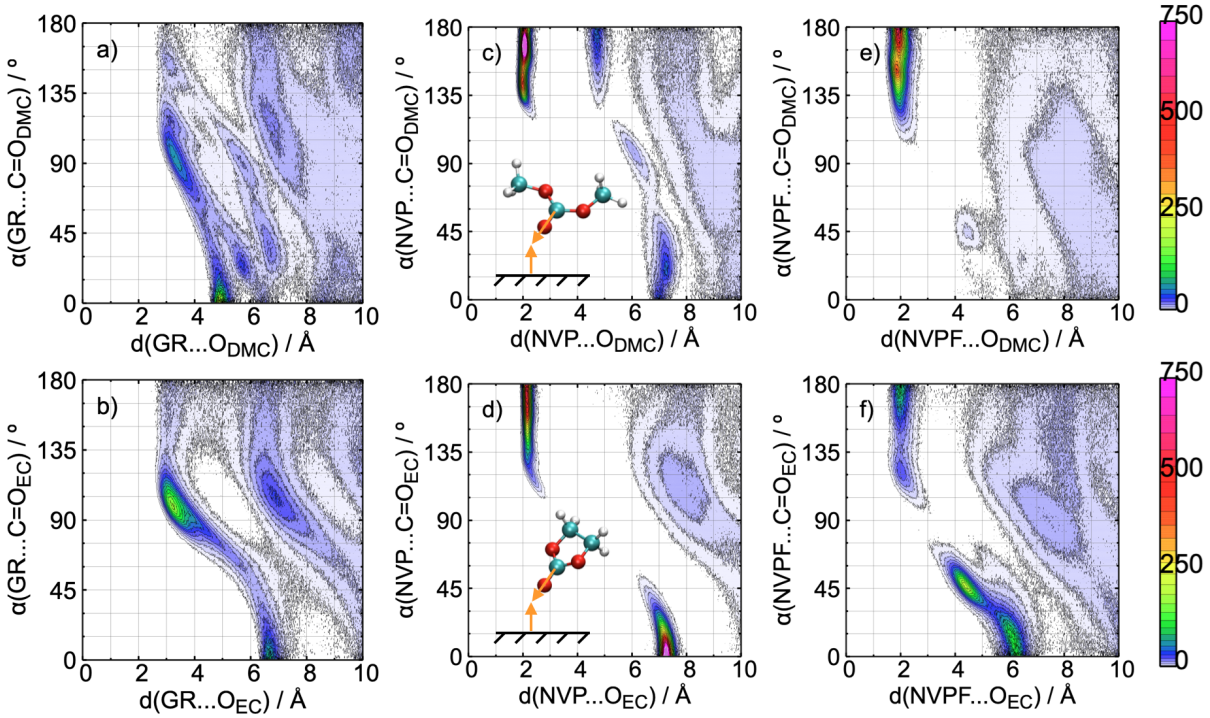

Figure 4: Probability contours revealing the orientation of the DMC and EC components in the 1 M $NaPF_6$/EC-DMC solution with respect to the electrode surface. The x-axes represent the distances between the electrode (top C for the graphite, top Na for the NVP and NVPF considered as a reference) and the O atoms of the carbonyl group of a solvent. The y-axis represents the angles formed by the normal vector to an electrode plane and the C=O vector of a solvent, as illustrated by the inset.

a function of their distance from an electrode, show that the local arrangement of a solvent at the graphite, NVP, and NVPF surfaces is considerably different. Being a non-polar material with a flat homogeneous surface, graphite seems not to have strong interactions with any of the solvents. Oxygen atoms of both DMC and EC of the EC-DMC mixture can be found at about 3.2 Å and 6.6 Å from the graphite surface, as shown in Figure 3a, that is consistent with neat DMC and PC (Figure 3b). The behavior of a carbonate solvent at a given interface seems to be determined by its flexibility (linear DMC or cyclic EC and PC) and is almost not affected by the presence of a co-solvent. The orientation of the molecules with respect to the surface is analyzed by computing the angle α formed by the C=O vector of a solvent and the normal vector to the electrode plane as a function of the O distance from the electrode surface. In the solvent mixture, DMC tends to expose its methyl groups to the graphite

https://doi.org/10.26434/chemrxiv-2023-7d7tz **ORCID:** https://orcid.org/0000-0002-1753-491X Content not peer-reviewed by ChemRxiv. **License:** CC BY-NC-ND 4.0

surface (Figure S1a), so that the C=O vector points away from the surface, marked by a greenish spot at about 4.8 Å O-surface separation (Figure 4a). This peak can be attributed to the solvent-electrolyte interactions as has been proposed by Borodin *et al.*[66] in their study of $LiPF_6$/EC-DMC/graphite by the surface-sensitive Ångstrom resolution X-ray reflectivity and molecular dynamics simulations. A lower probability but wide spot is observed at about 3.2 Å, which corresponds to the parallel orientation of the C=O vector with respect to the surface plane. The ratio between these two peaks should depend on the electrolyte concentration in the solution.[66] The second and further solvent layers are not clearly marked due to the conformation flexibility of DMC, which results in a variety of possible orientations. The behavior of neat DMC solvent appears to be quite similar (Figure S2a). On the contrary, the EC molecules of the mixture are mainly oriented parallelly to the surface (corresponding to $\alpha = 90°$, shown in Figure 4b), at the O...surface separation of 3.2 Å. In addition to this, a low probably perpendicular orientation is observed at 6.6 Å distance. In the case of neat PC (Figures S2b), this perpendicular orientation does not emerge, being replaced by two peaks at 6.5–7.5 Å with a tilted orientation of the C=O vector. The second solvent layer of parallelly oriented carbonate molecules is well-defined both for EC in the mixture and the neat PC.

The arrangement of solvent molecules at the NVP surface is strikingly different from that at graphite. The NVP slab, used for simulations, was cut in a way so that the PO_4^{3-} and the Na^+ ions are exposed to a solution. We considered it the most likely case because the direction of the highest Na^+ diffusion in the solid[27] is now aligned with the z axis of our simulation box. The top sodium ions of the NVP is then considered as a reference ($z = 0$) for the corresponding density profiles. A prominent peak between the top Na^+ ions of the surface and O atoms of the carbonyl groups is observed at about 2.15 Å in all solvents (Figures 3c-d). The high intensity of this peak points to a tight packing of the solvent molecules near the electrode. The orientation of the C=O vector with respect to the surface plane is strictly perpendicular (Figures 4c-d and Figures S3c-d). For DMC in the EC-DMC mixture, several

https://doi.org/10.26434/chemrxiv-2023-7d7tz **ORCID:** https://orcid.org/0000-0002-1753-491X Content not peer-reviewed by ChemRxiv. **License:** CC BY-NC-ND 4.0

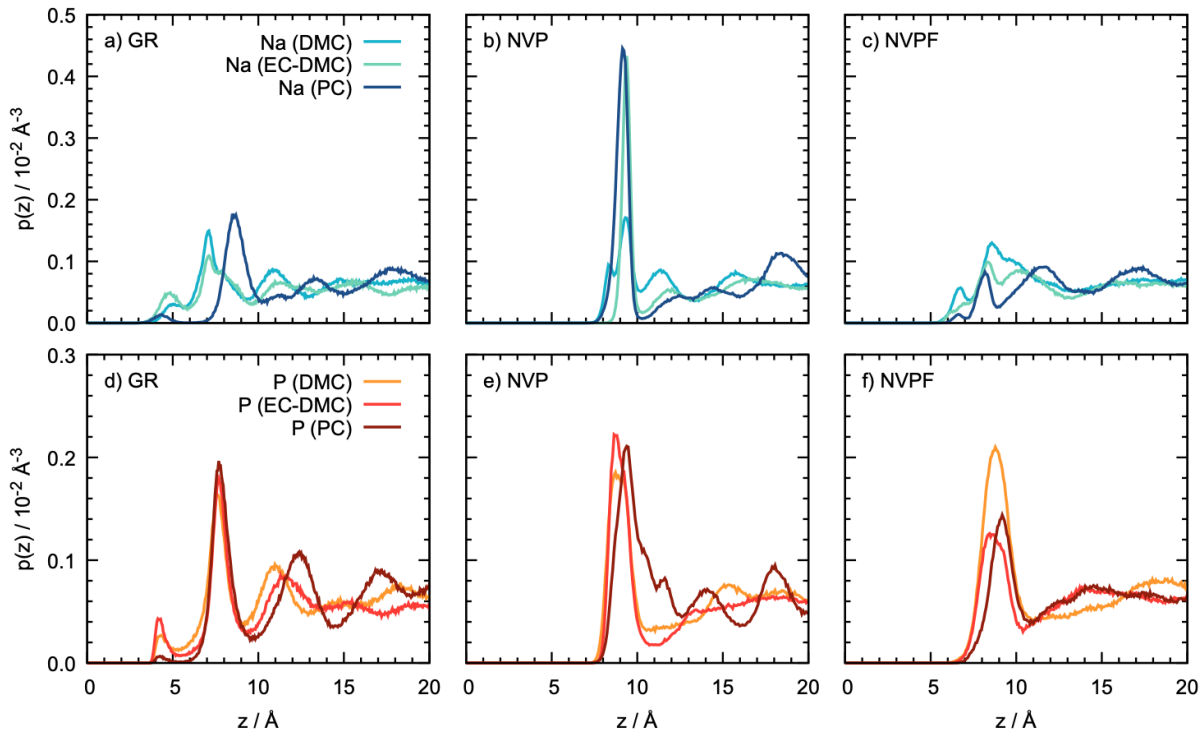

Figure 5: Density profiles of Na^+ ions (a-c) and P atoms (d-f) of the 1 M $NaPF_6$ salt in DMC, PC solvents (a-c), and the EC-DMC mixture (d-f) as a function of their distance from the graphite (a,d), NVP (b,e), and NVPF (c,f) electrodes. As a reference ($z = 0$), the top carbon layer of graphite and the top sodium ions of the NVP and NVPF are considered.

low-intense spots occur at 4.8 Å, 6.2 Å and 7.15 Å O...surface separations with different α values. On the contrary, in neat DMC, among these low-intensity contributions only that at 7.15 Å with C=O vector pointing away from the NVP plane is present. The probability of this peak increases when a cyclic carbonate is considered instead of a linear one: the intensity ratio between the peaks at 2.15 Å and 7.15 Å decreases from 17 for DMC to 2 for EC in the mixture. A similar effect was observed by Smith *et al.*[67] when modeling the $LiPF_6$/EC-DMC/$LiPO_4$ system: DMC molecules showed a slightly higher probability of interacting with alkali metal cations of the electrode, while EC molecules directed some of their hydrogen atoms towards O atoms at the surface.

Due to the presence of F atoms at the interface, the NVPF electrode appears to be more solvophobic than the NVP. The solvent molecules still interact with the top Na^+ ions,

https://doi.org/10.26434/chemrxiv-2023-7d7tz **ORCID:** https://orcid.org/0000-0002-1753-491X Content not peer-reviewed by ChemRxiv. **License:** CC BY-NC-ND 4.0

but the intensities of corresponding peaks are lower (Figures 3e-f). The DMC molecules are preferably oriented perpendicularly to the surface (α is close to 180°, Figures 4e): however, in the case of neat liquid (Figures S3e), the C=O is tilted from being completely perpendicular by about 15°. The latter allows the methyl groups of the solvent to undergo weak dispersion interactions with the F atoms at the surface. The cyclic carbonates exhibit three possible orientations (Figures 4f and Figures S3f): a first one which is perpendicular to the electrode, located at a characteristic distance of 2.1 Å, while the second one is further away from the electrode at an average distance of 6.1 Å. The third orientation is tilted, with $\alpha = 45°$ at 4.2 Å. The ratio between these orientations depends on the presence of a co-solvent. In the EC-DMC mixture, we observe a clear role splitting: while the linear carbonate interacts with top Na^+ ions of the surface, the C=O bond of the cyclic one is orientated towards the bulk solution. In the neat PC (Figures S3f), both roles are played by PC molecules in an equal proportion (evaluated by integrating the corresponding $p(z)$ peaks).

As was mentioned before, this notable fraction of solvent molecules oriented toward the bulk solution can be explained by the interactions with the $NaPF_6$ salt. In the case of graphite (Figure 5a), Na^+ ions are mainly found at about 7.1 Å from the electrode in the DMC and EC-DMC solutions, and at 8.6 Å in PC, being followed by several low-intensity peaks at larger separation. Since no tight solvent layer is present near the electrode, the Na^+ ions can approach the graphite even closer, being noticed at 4.4–4.8 Å separations. At the NVP electrode (Figure 5b), which exhibits strong solvent adsorption, an intense Na^+ peak is observed just after the first solvent layer, at about 9.2–9.4 Å. In the case of neat DMC, it is split into three smaller peaks (at 8.3 Å, 9.4 Å and 11.4 Å) due to multiple configurations of the flexible DMC molecule (Figures S3c), but the integral under them match that in EC/DMC and PC. At the NVPF surface (Figure 5c), the Na ions are distributed in the range of the 6.8–13.6 Å separations, with a principal peak at about 8.2–8.6 Å due to several dominant orientations of solvent molecules in the first layer(Figures 4e-f and Figures S3e-f).

While the sodium cation is small and densely charged, the PF_6^- anion is remarkably

https://doi.org/10.26434/chemrxiv-2023-7d7tz **ORCID:** https://orcid.org/0000-0002-1753-491X Content not peer-reviewed by ChemRxiv. **License:** CC BY-NC-ND 4.0

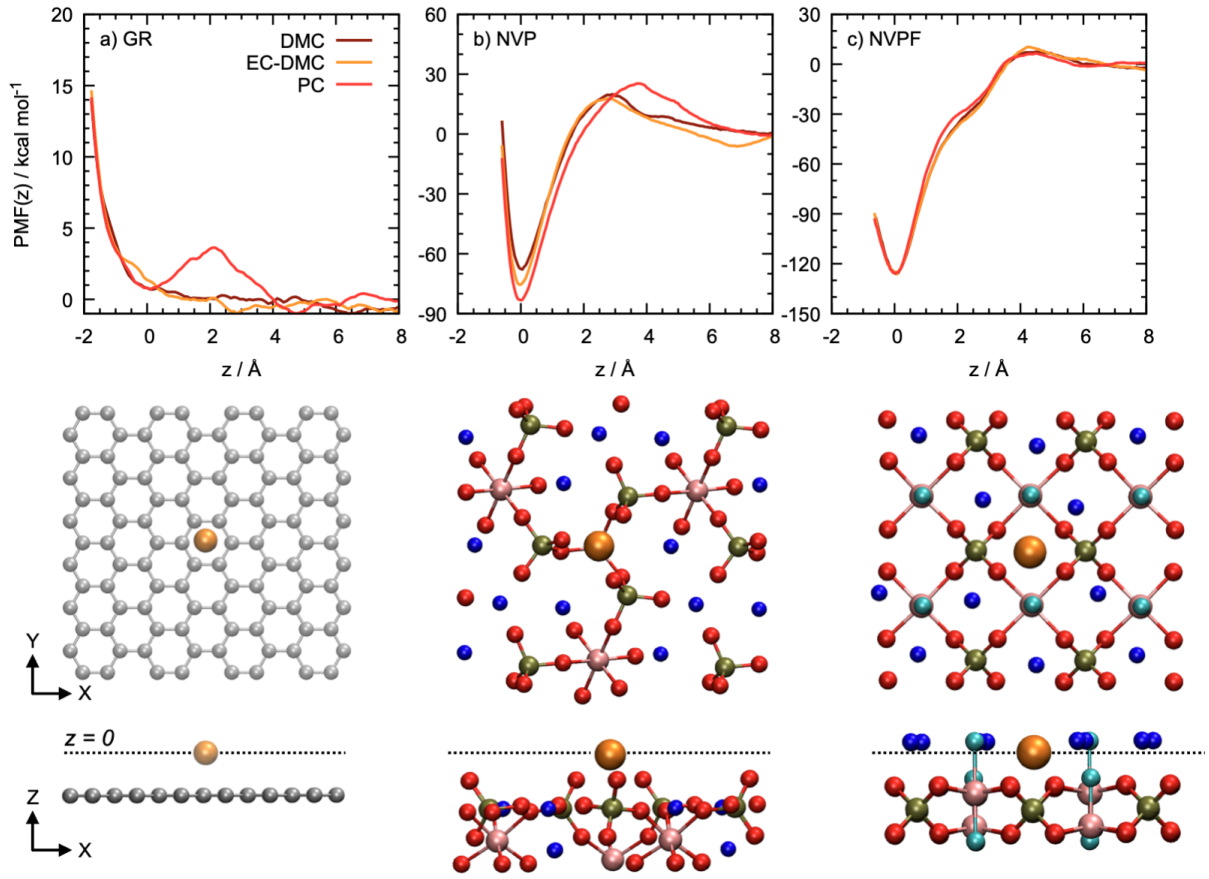

Figure 6: Potential of mean force of approaching a single Na^+ ion to the graphite (a), NVP (b), and NVPF (c) electrode in different solvents. As a reference ($z = 0$), the minimum of each PMF is considered, corresponding to the most energetically favorable position of the Na^+ ion, as illustrated by the simulation snapshots.

larger; it thus displays a lower charge density. Therefore, it is mainly located just after the first solvent layer at about 7.7 Å, 9.0 Å and 8.8 Å from the graphite, NVP and NVPF surfaces, respectively (Figure 5d-f). In all the solvents, the peak is high and well-defined due to the large anion size, which also allows us to clearly identify the second and sometimes third anionic layers, especially when neat rigid PC is used as a solvent. Similarly to the Na^+ cations, the PF_6^- anions can also approach the graphite surface closer, down to distances of about 4.2 Å, while no similar effects are observed in the NVP and NVPF cases.

The potential of mean force (PMF), the free energy profile as a function of the distance of a Na^+ ion relative to the electrode surface, can provide complementary information to

https://doi.org/10.26434/chemrxiv-2023-7d7tz ORCID: https://orcid.org/0000-0002-1753-491X Content not peer-reviewed by ChemRxiv. License: CC BY-NC-ND 4.0

the solvent arrangement.[68,69] Here, as a reference ($z = 0$), the distance corresponding to the minimum of each PMF is taken, being different from the density profile plots discussed earlier. Since there is no free energy barrier in approaching a Na^+ ion to the graphite surface in DMC or EC-DMC (Figure 6a), it can easily penetrate the closest solvent layer to the surface. This observation is consistent with the works of Hwang *et al.*[70] and Vatamanu *et al.*[71] on $LiPF_6$/EC-DMC/graphite system. On the contrary, a barrier of about 4.5 kcal mol^{-1} is observed in PC, probably related to a rigid geometry of the solvent molecules. This is reflected in the small prepeaks in density profiles, shown in Figure 5a, when the probability of observing a Na^+ ion near the surface is lower in neat PC than in other solvents. Due to the absence of specific sites at the graphite surface, capable of attracting the cation, it can freely move along and across the surface and move back to the bulk solution. Only in the case of PC, the barrier of about 3 kcal mol^{-1} should be overcome. In opposition to graphite, the NVP surface (Figure 6b) tends to form a firm solvent layer. In all the solvents, the free energy barrier attains about 20–25 kcal mol^{-1}. Once a cation reaches the NVP surface, it stays trapped there, being coordinated by three oxygen atoms of neighboring PO_4^{3-} groups, so that it is placed on the top of V atoms. The free energy of diffusing back to the solution appears to be too high (90–120 kcal mol^{-1}) to conquer.

The solvent layer at the NVPF surface is less tight, and the energy barrier achieves only 7–10 kcal mol^{-1}. The most probable adsorption site is in the hollow at the surface, being bounded by two oxygen atoms of PO_4^{3-} groups. In such a case, the cation starts to penetrate the electrode, and further investigation of this process becomes out of the scope of classical MD. Alternatively, Na^+ ions can be absorbed on the top of P atoms, stabilized by interaction with two oxygen atoms (Figure S4), when no hollow site is available nearby.

The origin of the free energy barrier rises from the partial desolvation of a Na^+ ion when it approaches the electrode, penetrating through a tight first solvent layer. This can be confirmed by tracking the coordination number of a single Na^+ ion moving towards the surface. Figure 7 (as well as Figure S5) shows that, indeed, no desolvation is observed

https://doi.org/10.26434/chemrxiv-2023-7d7tz **ORCID:** https://orcid.org/0000-0002-1753-491X Content not peer-reviewed by ChemRxiv. **License:** CC BY-NC-ND 4.0

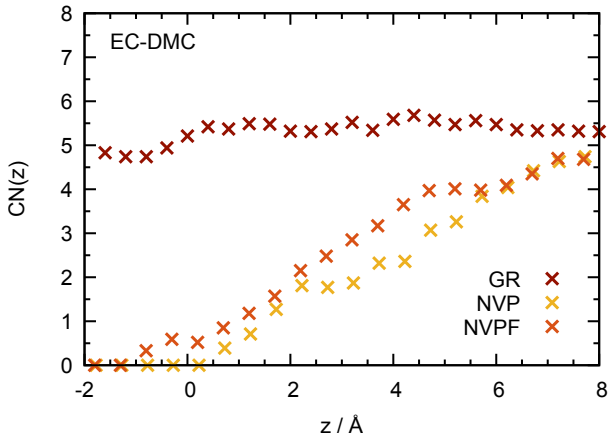

Figure 7: Total coordination number of solvent and anion species around a Na^+ cation moving towards the electrode surface in the $NaPF_6$/EC-DMC solution. As a reference ($z = 0$), the minimum of each PMF given Figure 6 is considered. The coordination number values are averaged over several replicas.

for the graphite, while the Na^+ cation loses its solvation shell when approaching NVP and NVPF. When comparing different materials, the firmness of solvent packing at a carbonate-based solvent at the electrode surface is greater at the NVP than at the NVPF, which actually explains the difference in the energy barriers: highly oriented solvent molecules at the interface require a higher energy contribution to change their configuration to solvate the diffusing Na^+ ion. In our recent EQCM study of the same systems under electrochemical cycling,[38] we observed a detectable mass loss right before the insertion of Na^+ ions related to the desolvation only at the NVP, while in the case of NVPF, due to loose packing, the desolvation process remains confined within the penetration depth of the resonator's acoustic wave, thus cannot be detected as a mass loss.

Quantitative and even qualitative comparison with literature data remains problematic since the value of the activation barrier depends on a diversity of factors. In addition, no data for Na^+-based systems have been reported to this point. Abe *et al.*[34,72] measured the activation barriers of $LiClO_4$ salt in DMC and EC−DMC (1:1 by vol.) at graphite by electrochemical impedance spectroscopy, and the variation between solvents (9.6 kcal mol^{-1} and 13.8 kcal mol^{-1} for DMC and EC−DMC, respectively) was explained by the lower solvation

https://doi.org/10.26434/chemrxiv-2023-7d7tz **ORCID:** https://orcid.org/0000-0002-1753-491X Content not peer-reviewed by ChemRxiv. **License:** CC BY-NC-ND 4.0

ability of DMC than that of EC. However, changing the nature of the SEI almost vanished the difference between the two solvents. In our theoretical model, no SEI is present and no barrier is observed for $NaPF_6$ in these two solvents near graphite. Nevertheless, the height of the free energy barrier (when present) should also depend on the nucleophilic properties of a solvent. In their experimental study of a SEI-free $LiPF_6/Li_4Ti_5O_{12}$ system, Xu *et al.*[36] showed that an ether-based electrolyte had lower desolvation energy (by about $3\,\mathrm{kcal\,mol^{-1}}$) than carbonates. By modelling the diffusion of a Li^+ ion towards $LiCoO_2$ in PC and water, Nikitina *et al.*[73] also obtained rather different values: $10.4\,\mathrm{kcal\,mol^{-1}}$ and $5.8\,\mathrm{kcal\,mol^{-1}}$, respectively. For our DMC - EC/DMC - PC carbonate series, the difference between solvents' donor ability is too delicate to be captured by simulations: partial changes of O solvent atoms are quite close and no explicit lone pairs are present. Therefore, the solvent packing at the interface appears to play the principal role in defining the height of the activation barrier.

4 Conclusions

To sum up, the diffusion of a Na^+ ion through the electrolyte solution towards the cathode is strongly dependent on the surface nature. The nanostructure of the closest solvent layer at the interface defines the height of the activation barrier, commonly associated with the desolvation process. The desolvation does not seem to be observed at the SEI-free graphite electrode due to the absence of specific directional interaction between the solvent and the carbon sheets. On the contrary, because of the surface inhomogeneity and the presence of donor and acceptor groups, the polyanionic Na-insertion compounds exhibit a notable arrangement of solvent molecules in the closest layer, penetrating through which a Na^+ ion partially loses its solvent shell. The effect is the most pronounced at the NVP, which demonstrates the greatest energy barrier among studied systems as a result of the highly ordered and well-oriented first solvent layer. The solvent arrangement at the NVPF surface

https://doi.org/10.26434/chemrxiv-2023-7d7tz **ORCID:** https://orcid.org/0000-0002-1753-491X Content not peer-reviewed by ChemRxiv. **License:** CC BY-NC-ND 4.0

is slightly less marked due to the presence of non-polar fluorine atoms which partially disturb the solvent-electrode electrostatic attraction.

The nature of the solvent also plays an important role, but only when different families of solvents are compared. In our carbonate series, the variation between solvents (namely, due to the partial charge distribution) is quite subtle being a less significant factor than the electrode material. Even so, the lack of flexibility of the solvent impacts the tightness of its packing at the surface, which can lead to an increase in the activation energy barrier.

Acknowledgement

This work was funded by the European Research Council (ERC) under the European Union Horizon 2020 research and innovation program (grant agreement 771294). Computational tasks were performed using resources from GENCI-IDRIS (Grants 2022-A0120910463 and 2023-A0140910463) and from the MeSU supercomputer of Sorbonne University.

Supporting Information Available

Density profiles, probability contours, simulation snapshots, and coordination number plots.

References

(1) Armand, M.; Tarascon, J. M. Building better batteries. *Nature* **2008**, *451*, 652–657, DOI: 10.1038/451652a.

(2) Li, M.; Lu, J.; Chen, Z.; Amine, K. 30 Years of Lithium-Ion Batteries. *Adv. Mater.* **2018**, *30*, 1800561, DOI: 10.1002/adma.201800561.

(3) Kim, T.; Song, W.; Son, D.-Y.; Ono, L. K.; Qi, Y. Lithium-ion batteries: outlook on

https://doi.org/10.26434/chemrxiv-2023-7d7tz **ORCID:** https://orcid.org/0000-0002-1753-491X Content not peer-reviewed by ChemRxiv. **License:** CC BY-NC-ND 4.0

present, future, and hybridized technologies. *J. Mater. Chem. A* **2019**, *7*, 2942–2964, DOI: 10.1039/C8TA10513H.

(4) Yabuuchi, N.; Kubota, K.; Dahbi, M.; Komaba, S. Research Development on Sodium-Ion Batteries. *Chem. Rev.* **2014**, *114*, 11636–11682, DOI: 10.1021/cr500192f.

(5) Goikolea, E.; Palomares, V.; Wang, S.; de Larramendi, I. R.; Guo, X.; Wang, G.; Rojo, T. Na-Ion Batteries—Approaching Old and New Challenges. *Adv. Energy Mater.* **2020**, *10*, 2002055, DOI: 10.1002/aenm.202002055.

(6) Chayambuka, K.; Mulder, G.; Danilov, D. L.; Notten, P. H. L. Sodium-Ion Battery Materials and Electrochemical Properties Reviewed. *Adv. Energy Mater.* **2018**, *8*, 1800079, DOI: 10.1002/aenm.201800079.

(7) Hwang, J.-Y.; Myung, S.-T.; Sun, Y.-K. Sodium-ion batteries: present and future. *Chem. Soc. Rev.* **2017**, *46*, 3529–3614, DOI: 10.1039/C6CS00776G.

(8) Nayak, P. K.; Yang, L.; Brehm, W.; Adelhelm, P. From Lithium-Ion to Sodium-Ion Batteries: Advantages, Challenges, and Surprises. *Angew. Chem., Int. Ed.* **2018**, *57*, 102–120, DOI: 10.1002/anie.201703772.

(9) Palomares, V.; Serras, P.; Villaluenga, I.; Hueso, K. B.; Carretero-González, J.; Rojo, T. Na-ion batteries, recent advances and present challenges to become low cost energy storage systems. *Energy Environ. Sci.* **2012**, *5*, 5884–5901, DOI: 10.1039/C2EE02781J.

(10) Masquelier, C.; Croguennec, L. Polyanionic (Phosphates, Silicates, Sulfates) Frameworks as Electrode Materials for Rechargeable Li (or Na) Batteries. *Chem. Rev.* **2013**, *113*, 6552–6591, DOI: 10.1021/cr3001862.

(11) Singh, B.; Wang, Z.; Park, S.; Gautam, G. S.; Chotard, J.-N.; Croguennec, L.; Carlier, D.; Cheetham, A. K.; Masquelier, C.; Canepa, P. A chemical map of NaSICON electrode materials for sodium-ion batteries. *J. Mater. Chem. A* **2021**, *9*, 281–292.

https://doi.org/10.26434/chemrxiv-2023-7d7tz **ORCID:** https://orcid.org/0000-0002-1753-491X Content not peer-reviewed by ChemRxiv. **License:** CC BY-NC-ND 4.0

(12) Goodenough, J. B.; Hong, H. Y.-P.; Kafalas, J. A. Fast Na+-ion transport in skeleton structures. *Mater. Res. Bull.* **1976**, *11*, 203–220, DOI: 10.1016/0025-5408(76)90077-5.

(13) Shen, X.; Su, Y.; Yang, N.; Jiang, X.; Liu, X.; Mo, J.; Ran, Y.; Wu, F. Na+-Activation Engineering in the Na3V2(PO4)3 Cathode with Boosting Kinetics for Fast-Charging Na-Ion Batteries. *ACS Appl. Mater. Interfaces* **2022**, *14*, 47685–47695.

(14) Jin, T.; Li, H.; Zhu, K.; Wang, P.-F.; Liu, P.; Jiao, L. Polyanion-type cathode materials for sodium-ion batteries. *Chem. Soc. Rev.* **2020**, *49*, 2342–2377, DOI: 10.1039/C9CS00846B.

(15) Cheng, J.; Chen, Y.; Sun, S.; Tian, Z.; Linghu, Y.; Tian, Z.; Wang, C.; He, Z.; Guo, L. Na3V2(PO4)3/C·Na3V2(PO4)2F3/C@rGO blended cathode material with elevated energy density for sodium ion batteries. *Ceram. Int.* **2021**, *47*, 18065–18074, DOI: 10.1016/j.ceramint.2021.03.122.

(16) Yang, Z.; Li, G.; Sun, J.; Xie, L.; Jiang, Y.; Huang, Y.; Chen, S. High performance cathode material based on Na3V2(PO4)2F3 and Na3V2(PO4)3 for sodium-ion batteries. *Energy Stor. Mater.* **2020**, *25*, 724–730, DOI: 10.1016/j.ensm.2019.09.014.

(17) Ponrouch, A.; Dedryvère, R.; Monti, D.; Demet, A. E.; Ateba Mba, J. M.; Croguennec, L.; Masquelier, C.; Johansson, P.; Palacín, M. R. Towards high energy density sodium ion batteries through electrolyte optimization. *Energy & Environmental Science* **2013**, *6*, 2361–2369, DOI: 10.1039/C3EE41379A.

(18) Ponrouch, A.; Monti, D.; Boschin, A.; Steen, B.; Johansson, P.; Palacín, M. R. Non-aqueous electrolytes for sodium-ion batteries. *J. Mater. Chem. A* **2015**, *3*, 22–42, DOI: 10.1039/C4TA04428B.

(19) Heinz, H.; Vaia, R. A.; Farmer, B. L.; Naik, R. R. Accurate Simulation of Surfaces and

https://doi.org/10.26434/chemrxiv-2023-7d7tz **ORCID:** https://orcid.org/0000-0002-1753-491X Content not peer-reviewed by ChemRxiv. **License:** CC BY-NC-ND 4.0

Interfaces of Face-Centered Cubic Metals Using 12-6 and 9-6 Lennard-Jones Potentials. *J. Phys. Chem. C* **2008**, *112*, 17281–17290, DOI: 10.1021/jp801931d.

(20) Yan, G.; Reeves, K.; Foix, D.; Li, Z.; Cometto, C.; Mariyappand, S.; Salanne, M.; Tarascon, J.-M. A New Electrolyte Formulation for Securing High Temperature Cycling and Storage Performances of Na-Ion Batteries. *Adv. Ener. Mater.* **2019**, *9*, 1901431.

(21) Hijazi, H.; Desai, P.; Mariyappan, S. Non-Aqueous Electrolytes for Sodium-Ion Batteries: Challenges and Prospects Towards Commercialization. *Batter. Supercaps* **2021**, *4*, 881–896, DOI: 10.1002/batt.202000277.

(22) Muñoz-Márquez, M. Á.; Zarrabeitia, M.; Passerini, S.; Rojo, T. Structure, Composition, Transport Properties, and Electrochemical Performance of the Electrode-Electrolyte Interphase in Non-Aqueous Na-Ion Batteries. *Adv. Mater. Interfaces* **2022**, *9*, 2101773, DOI: 10.1002/admi.202101773.

(23) Gomes Chagas, L.; Jeong, S.; Hasa, I.; Passerini, S. Ionic Liquid-Based Electrolytes for Sodium-Ion Batteries: Tuning Properties To Enhance the Electrochemical Performance of Manganese-Based Layered Oxide Cathode. *ACS Appl. Mater. Interfaces* **2019**, *11*, 22278–22289.

(24) Liu, T.; Wu, H.; Du, X.; Wang, J.; Chen, Z.; Wang, H.; Sun, J.; Zhang, J.; Niu, J.; Yao, L. *et al.* Water-Locked Eutectic Electrolyte Enables Long-Cycling Aqueous Sodium-Ion Batteries. *ACS Appl. Mater. Interfaces* **2022**, *14*, 33041–33051.

(25) Yang, Q.; Zhang, Z.; Sun, X.-G.; Hu, Y.-S.; Xing, H.; Dai, S. Ionic liquids and derived materials for lithium and sodium batteries. *Chem. Soc. Rev.* **2018**, *47*, 2020–2064, DOI: 10.1039/C7CS00464H.

(26) Kim, H.; Hong, J.; Park, K.-Y.; Kim, H.; Kim, S.-W.; Kang, K. Aqueous Rechargeable Li and Na Ion Batteries. *Chem. Rev.* **2014**, *114*, 11788–11827, DOI: 10.1021/cr500232y.

https://doi.org/10.26434/chemrxiv-2023-7d7tz **ORCID:** https://orcid.org/0000-0002-1753-491X Content not peer-reviewed by ChemRxiv. **License:** CC BY-NC-ND 4.0

(27) Chotard, J.-N.; Rousse, G.; David, R.; Mentré, O.; Courty, M.; Masquelier, C. Discovery of a Sodium-Ordered Form of Na3V2(PO4)3 below Ambient Temperature. *Chem. Mater.* **2015**, *27*, 5982–5987, DOI: 10.1021/acs.chemmater.5b02092.

(28) Bianchini, M.; Brisset, N.; Fauth, F.; Weill, F.; Elkaim, E.; Suard, E.; Masquelier, C.; Croguennec, L. Na3V2(PO4)2F3 Revisited: A High-Resolution Diffraction Study. *Chem. Mater.* **2014**, *26*, 4238–4247, DOI: 10.1021/cm501644g.

(29) Bui, K. M.; Dinh, V. A.; Okada, S.; Ohno, T. Hybrid functional study of the NASICON-type Na3V2(PO4)3: crystal and electronic structures, and polaron–Na vacancy complex diffusion. *Phys. Chem. Chem. Phys.* **2015**, *17*, 30433–30439, DOI: 10.1039/C5CP05323D.

(30) Wang, Q.; Zhang, M.; Zhou, C.; Chen, Y. Concerted Ion-Exchange Mechanism for Sodium Diffusion and Its Promotion in Na3V2(PO4)3 Framework. *J. Phys. Chem. C* **2018**, *122*, 16649–16654, DOI: 10.1021/acs.jpcc.8b06120.

(31) Song, W.; Ji, X.; Wu, Z.; Zhu, Y.; Yang, Y.; Chen, J.; Jing, M.; Li, F.; Banks, C. E. First exploration of Na-ion migration pathways in the NASICON structure Na3V2(PO4)3. *J. Mater. Chem. A* **2014**, *2*, 5358–5362, DOI: 10.1039/C4TA00230J.

(32) Broux, T.; Fleutot, B.; David, R.; Brüll, A.; Veber, P.; Fauth, F.; Courty, M.; Croguennec, L.; Masquelier, C. Temperature Dependence of Structural and Transport Properties for Na3V2(PO4)2F3 and Na3V2(PO4)2F2.5O0.5. *Chem. Mater.* **2018**, *30*, 358–365.

(33) Park, S.; Wang, Z.; Deng, Z.; Moog, I.; Canepa, P.; Fauth, F.; Carlier, D.; Croguennec, L.; Masquelier, C.; Chotard, J.-N. Crystal Structure of Na2V2(PO4)3, an Intriguing Phase Spotted in the Na3V2(PO4)3–Na1V2(PO4)3 System. *Chem. Mater.* **2022**, *34*, 451–462, DOI: 10.1021/acs.chemmater.1c04033.

(34) Abe, T.; Fukuda, H.; Iriyama, Y.; Ogumi, Z. Solvated Li-Ion Transfer at Interface

https://doi.org/10.26434/chemrxiv-2023-7d7tz **ORCID:** https://orcid.org/0000-0002-1753-491X Content not peer-reviewed by ChemRxiv. **License:** CC BY-NC-ND 4.0

Between Graphite and Electrolyte. *J. Electrochem. Soc.* **2004**, *151*, A1120, DOI: 10.1149/1.1763141.

(35) Abe, T.; Sagane, F.; Ohtsuka, M.; Iriyama, Y.; Ogumi, Z. Lithium-Ion Transfer at the Interface Between Lithium-Ion Conductive Ceramic Electrolyte and Liquid Electrolyte-A Key to Enhancing the Rate Capability of Lithium-Ion Batteries. *J. Electrochem. Soc.* **2005**, *152*, A2151, DOI: 10.1149/1.2042907.

(36) Xu, K.; von Cresce, A.; Lee, U. Differentiating Contributions to "Ion Transfer"Barrier from Interphasial Resistance and Li+ Desolvation at Electrolyte/Graphite Interface. *Langmuir* **2010**, *26*, 11538–11543, DOI: 10.1021/la1009994.

(37) Jeanmairet, G.; Rotenberg, B.; Salanne, M. Microscopic Simulations of Electrochemical Double-Layer Capacitors. *Chem. Rev.* **2022**, in press, DOI: 10.1021/acs.chemrev.1c00925.

(38) Bendadesse, E.; Gervillié-Mouravieff, C.; Leau, C.; Goloviznina, K.; Rabuel, F.; Salanne, M.; Tarascon, J.-M.; Sel, O. Spotting Interface Structuring during Na-Insertion into the NaSICON Na3V2(PO4)3 by EQCM and Operando Fiber Optic Infrared Spectroscopy. *Advanced Energy Materials* **2023**, 2300930, DOI: 10.1002/aenm.202300930.

(39) Lemaire, P.; Serva, A.; Salanne, M.; Rousse, G.; Perrot, H.; Sel, O.; Tarascon, J.-M. Probing the Electrode–Electrolyte Interface of a Model K-Ion Battery Electrode - The Origin of Rate Capability Discrepancy between Aqueous and Non-Aqueous Electrolytes. *ACS Appl. Mater. Interfaces* **2022**, *14*, 20835–20847.

(40) Plimpton, S. J. Fast Parallel Algorithms for Short-Range Molecular Dynamics. *J. Comput. Phys.* **1995**, *117*, 1–19, DOI: 10.1006/jcph.1995.1039.

(41) Martínez, L.; Andrade, R.; Birgin, E. G.; Martínez, J. M. PACKMOL: A package for building initial configurations for molecular dynamics simulations. *J. Comp. Chem.* **2009**, *30*, 2157–2164, DOI: 10.1002/jcc.21224.

https://doi.org/10.26434/chemrxiv-2023-7d7tz **ORCID:** https://orcid.org/0000-0002-1753-491X Content not peer-reviewed by ChemRxiv. **License:** CC BY-NC-ND 4.0

(42) Momma, K.; Izumi, F. VESTA: a three-dimensional visualization system for electronic and structural analysis. *J. Appl. Crystallogr.* **2008**, *41*, 653–658, DOI: 10.1107/S0021889808012016.

(43) Padua, A. A. H. github.com/paduagroup/fftool. 2022; https://github.com/paduagroup/fftool, (accessed 18 October 2022).

(44) Trucano, P.; Chen, R. Structure of graphite by neutron diffraction. *Nature* **1975**, *258*, 136–137, DOI: 10.1038/258136a0.

(45) Zatovsky, I. V. NASICON-type $Na_3V_2(PO_4)_3$. *Acta Crystallogr. E: Crystallogr. Commun.* **2010**, *66*, i12, DOI: 10.1107/S1600536810002801.

(46) Ghosh, S.; Barman, N.; Mazumder, M.; Pati, S. K.; Rousse, G.; Senguttuvan, P. High Capacity and High-Rate NASICON-Na3.75V1.25Mn0.75(PO4)3 Cathode for Na-Ion Batteries via Modulating Electronic and Crystal Structures. *Adv. Energy Mater.* **2020**, *10*, 1902918, DOI: 10.1002/aenm.201902918.

(47) Chen, M.; Hua, W.; Xiao, J.; Zhang, J.; Lau, V. W.-h.; Park, M.; Lee, G.-H.; Lee, S.; Wang, W.; Peng, J. *et al.* Activating a Multielectron Reaction of NASICON-Structured Cathodes toward High Energy Density for Sodium-Ion Batteries. *J. Am. Chem. Soc.* **2021**, *143*, 18091–18102, DOI: 10.1021/jacs.1c06727.

(48) Le Meins, J. M.; Crosnier-Lopez, M. P.; Hemon-Ribaud, A.; Courbion, G. Phase Transitions in the Na3M2(PO4)2F3 Family (M=Al3+, V3+, Cr3+, Fe3+, Ga3+): Synthesis, Thermal, Structural, and Magnetic Studies. *J. Solid State Chem.* **1999**, *148*, 260–277, DOI: 10.1006/jssc.1999.8447.

(49) Shakoor, R. A.; Seo, D.-H.; Kim, H.; Park, Y.-U.; Kim, J.; Kim, S.-W.; Gwon, H.; Lee, S.; Kang, K. A combined first principles and experimental study on Na3V2(PO4)2F3 for rechargeable Na batteries. *J. Mater. Chem.* **2012**, *22*, 20535–20541, DOI: 10.1039/C2JM33862A.

https://doi.org/10.26434/chemrxiv-2023-7d7tz **ORCID:** https://orcid.org/0000-0002-1753-491X Content not peer-reviewed by ChemRxiv. **License:** CC BY-NC-ND 4.0

(50) Suh, I.-K.; Ohta, H.; Waseda, Y. High-temperature thermal expansion of six metallic elements measured by dilatation method and X-ray diffraction. *J. Mater. Sci.* **1988**, *23*, 757–760, DOI: 10.1007/BF01174717.

(51) Åqvist, J. Ion-water interaction potentials derived from free energy perturbation simulations. *J. Phys. Chem.* **1990**, *94*, 8021–8024, DOI: 10.1021/j100384a009.

(52) Canongia Lopes, J. N.; Deschamps, J.; Pádua, A. A. H. Modeling Ionic Liquids Using a Systematic All-Atom Force Field. *J. Phys. Chem. B* **2004**, *108*, 2038–2047, DOI: 10.1021/jp0362133.

(53) Padua, A. A. H. github.com/paduagroup/clandp. 2022; https://github.com/paduagroup/clandp, (accessed 18 October 2022).

(54) Cole, M. W.; Klein, J. R. The interaction between noble gases and the basal plane surface of graphite. *Surf. Sci.* **1983**, *124*, 547–554, DOI: 10.1016/0039-6028(83)90808-7.

(55) Gupta, S.; Wai, N.; Lim, T. M.; Mushrif, S. H. Force-field parameters for vanadium ions (+2, +3, +4, +5) to investigate their interactions within the vanadium redox flow battery electrolyte solution. *J. Mol. Liq.* **2016**, *215*, 596–602, DOI: 10.1016/j.molliq.2016.01.028.

(56) Murzyn, K.; Bratek, M.; Pasenkiewicz-Gierula, M. Refined OPLS All-Atom Force Field Parameters for n-Pentadecane, Methyl Acetate, and Dimethyl Phosphate. *J. Phys. Chem. B* **2013**, *117*, 16388–16396, DOI: 10.1021/jp408162d.

(57) Horinek, D.; Mamatkulov, S. I.; Netz, R. R. Rational design of ion force fields based on thermodynamic solvation properties. *J. Chem. Phys.* **2009**, *130*, 124507, DOI: 10.1063/1.3081142.

(58) Jorgensen, W. L.; Maxwell, D. S.; Tirado-Rives, J. Development and Testing of the

https://doi.org/10.26434/chemrxiv-2023-7d7tz **ORCID:** https://orcid.org/0000-0002-1753-491X Content not peer-reviewed by ChemRxiv. **License:** CC BY-NC-ND 4.0

OPLS All-Atom Force Field on Conformational Energetics and Properties of Organic Liquids. *J. Am. Chem. Soc.* **1996**, *118*, 11225–11236.

(59) Breneman, C. M.; Wiberg, K. B. Determining atom-centered monopoles from molecular electrostatic potentials. The need for high sampling density in formamide conformational analysis. *J. Comput. Chem.* **1990**, *11*, 361–373, DOI: 10.1002/jcc.540110311.

(60) Frisch, M. J.; Trucks, G. W.; Schlegel, H. B.; Scuseria, G. E.; Robb, M. A.; Cheeseman, J. R.; Scalmani, G.; Barone, V.; Petersson, G. A.; Nakatsuji, H. *et al.* Gaussian˜16 Revision B.01. 2016; https://gaussian.com/gaussian16/, Gaussian Inc. Wallingford CT.

(61) Brehm, M.; Kirchner, B. TRAVIS - A Free Analyzer and Visualizer for Monte Carlo and Molecular Dynamics Trajectories. *J. Chem. Inf. Model.* **2011**, *51*, 2007–2023, DOI: 10.1021/ci200217w.

(62) Brehm, M.; Thomas, M.; Gehrke, S.; Kirchner, B. TRAVIS—A free analyzer for trajectories from molecular simulation. *J. Chem. Phys.* **2020**, *152*, 164105, DOI: 10.1063/5.0005078.

(63) Humphrey, W.; Dalke, A.; Schulten, K. VMD: Visual molecular dynamics. *J. Mol. Graph.* **1996**, *14*, 33–38, DOI: 10.1016/0263-7855(96)00018-5.

(64) Kumar, S.; Rosenberg, J. M.; Bouzida, D.; Swendsen, R. H.; Kollman, P. A. The weighted histogram analysis method for free-energy calculations on biomolecules. I. The method. *J. Comput. Chem.* **1992**, *13*, 1011–1021, DOI: 10.1002/jcc.540130812.

(65) Grossfield, A. WHAM: the weighted histogram analysis method. 2021; http://membrane.urmc.rochester.edu/?page_id=126, (accessed 15 February 2023).

(66) Steinrück, H.-G.; Cao, C.; Tsao, Y.; Takacs, C. J.; Konovalov, O.; Vatamanu, J.;

https://doi.org/10.26434/chemrxiv-2023-7d7tz **ORCID:** https://orcid.org/0000-0002-1753-491X Content not peer-reviewed by ChemRxiv. **License:** CC BY-NC-ND 4.0

Borodin, O.; Toney, M. F. The nanoscale structure of the electrolyte–metal oxide interface. *Energy Environ. Sci.* **2018**, *11*, 594–602, DOI: 10.1039/C7EE02724A.

(67) Smith, G. D.; Borodin, O.; Russo, S. P.; Rees, R. J.; Hollenkamp, A. F. A molecular dynamics simulation study of LiFePO4/electrolyte interfaces: structure and Li+ transport in carbonate and ionic liquid electrolytes. *Phys. Chem. Chem. Phys.* **2009**, *11*, 9884–9897, DOI: 10.1039/B912820D.

(68) Dubouis, N.; Serva, A.; Berthin, R.; Jeanmairet, G.; Porcheron, B.; Salager, E.; Salanne, M.; Grimaud, A. Tuning water reduction through controlled nanoconfinement within an organic liquid matrix. *Nat. Catal.* **2020**, *3*, 656–663.

(69) Dorchies, F.; Serva, A.; Crevel, D.; De Freitas, J.; Kostopoulos, N.; Robert, M.; Sel, O.; Salanne, M.; Grimaud, A. Controlling the Hydrophilicity of the Electrochemical Interface to Modulate the Oxygen-Atom Transfer in Electrocatalytic Epoxidation Reactions. *J. Am. Chem. Soc.* **2022**, *144*, 22734–22746.

(70) Boyer, M. J.; Vilčiauskas, L.; Hwang, G. S. Structure and Li+ ion transport in a mixed carbonate/LiPF6 electrolyte near graphite electrode surfaces: a molecular dynamics study. *Phys. Chem. Chem. Phys.* **2016**, *18*, 27868–27876, DOI: 10.1039/C6CP05140E.

(71) Vatamanu, J.; Borodin, O.; Smith, G. D. Molecular Dynamics Simulation Studies of the Structure of a Mixed Carbonate/LiPF6 Electrolyte near Graphite Surface as a Function of Electrode Potential. *J. Phys. Chem. C* **2012**, *116*, 1114–1121, DOI: 10.1021/jp2101539.

(72) Yamada, Y.; Iriyama, Y.; Abe, T.; Ogumi, Z. Kinetics of Lithium Ion Transfer at the Interface between Graphite and Liquid Electrolytes: Effects of Solvent and Surface Film. *Langmuir* **2009**, *25*, 12766–12770, DOI: 10.1021/la901829v.

(73) Chekushkin, P. M.; Merenkov, I. S.; Smirnov, V. S.; Kislenko, S. A.; Nikitina, V. A. The physical origin of the activation barrier in Li-ion intercalation processes: the

https://doi.org/10.26434/chemrxiv-2023-7d7tz **ORCID:** https://orcid.org/0000-0002-1753-491X Content not peer-reviewed by ChemRxiv. **License:** CC BY-NC-ND 4.0

overestimated role of desolvation. *Electrochim. Acta* **2021**, *372*, 137843, DOI: 10.1016/j.electacta.2021.137843.

https://doi.org/10.26434/chemrxiv-2023-7d7tz **ORCID:** https://orcid.org/0000-0002-1753-491X Content not peer-reviewed by ChemRxiv. **License:** CC BY-NC-ND 4.0